Engineering Geology 296 (2022) 106439

Contents lists available at ScienceDirect

Engineering Geology

journal homepage: www.elsevier.com/locate/enggeo

New data on the microporosity of bentonites

Mercedes Suárez [a,*], Adrián Lorenzo [a], Andrea García-Vicente [a], Juan Morales [a], Javier García-Rivas [a], Emilia García-Romero [b,c]

[a] Department of Geology, University of Salamanca, Plaza de la Merced s/n, Salamanca 37008, Spain
[b] Department of Mineralogy and Petrology, Complutense University of Madrid, C/José Antonio Novais 12, Madrid 28040, Spain
[c] Geosciences Institute, Spanish Research Council and Complutense University of Madrid, C/José Antonio Novais 12, Madrid 28040, Spain

ARTICLE INFO

Keywords:
Bentonite
Smectites
Specific surface area
Microporosity
Microstructure

ABSTRACT

This comparative study on a very wide group of samples shows that the crystal size and crystalline defects of smectites influence microporosity of bentonite considerably more than previously considered. The smectite crystals and surface properties, including microporosity and micropore volume, were studied using high resolution transmission electron microscopy and N_2 adsorption, respectively. The specific surface area obtained varied between 25 and 278 m^2g^{-1}. The micropore area ranged between 6 and 76 m^2g^{-1}, and the external area ranged from 18 to 208 m^2g^{-1}. The external surface area was related to the size of the crystals in [001] direction because of the smaller particles with few stacked 2:1 layers have more basal surfaces accessible to the N_2 molecules. However, the microporosity can be related to 1) the size of the crystals, owing to the partial ability of N_2 to penetrate into the interlayer space, 2) the abundance of crystalline defects affecting the stacking of the 2:1 layers, and 3) the arrangement of the crystals forming particles, in which sub-parallel aggregates generate micro and mesopores. The study shows that these bentonites have pores in the full range, from smaller micropores (related to the crystalline structure in the interior of the interlayer) to micrometric macropores. The amounts of micro, *meso*, and macropores varied between samples but were similar and characteristic for samples from the same geological area.

1. Introduction

Bentonites are clayey rocks formed by minerals from the smectite group: montmorillonite, beidellite, and saponite, mainly. They have strong interest because of their swelling property that may be a significant hazard to engineering construction (Jones and Jefferson, 2012; Adem and Vanapalli, 2015, among others). Furthermore, due to this swelling property, low permeability, and high adsorption capacity, compacted bentonite has been proposed as candidate engineering buffer material for disposal of radioactive waste in deep geological repositories (Villar and Lloret, 2004; Zhang et al., 2016). On the other hand, bentonites are probably the mineral resources with the widest range of applications within industrial minerals, and they can be subjected to modifications after different treatments, such as acid and base attack (Jeon and Nam, 2019), intercalation (Okada et al., 2014), and pillaring (Kloprogge et al., 2005; Vicente et al., 2013), to improve some of their natural properties. Both natural and treated bentonites are used for the synthesis of organo-complexes (Komadel et al., 2005) and clay-polymer nanocomposites (Jlassi et al., 2017), and in environmental remediation (Vicente et al., 2010; Yamada et al., 2011). All these sectors benefit from several properties, including the swelling, rheological properties, cation exchange capacity (CEC), and the surface properties including microporosity.

Both for geotechnics and for the industrial application of bentonites, the knowledge of the porosity is essential. The porosity of bentonites covers the full range from microporosity to macroporosity (Přikryl and Weishauptová, 2010; Sun et al., 2020; Navarro et al., 2020) but it is concentrated at lower pore sizes: micro and mesopores. The smaller porosity is useful for adsorption processes and it is related to the specific surface area. The specific surface area of bentonites is influenced by their microporosity and is largely variable and can be determined by various methods. It can be estimated from the average dimensions of the individual smectite layers, from the absorption of methylene blue in aqueous suspension, and from adsorption of gases, mainly nitrogen. The method using the absorption of methylene blue primarily measures the internal surface area, whereas the BET method (Brunauer et al., 1938)

* Corresponding author.
E-mail address: msuarez@usal.es (M. Suárez).

https://doi.org/10.1016/j.enggeo.2021.106439
Received 25 March 2021; Received in revised form 21 June 2021; Accepted 21 October 2021
Available online 25 October 2021
0013-7952/© 2021 Published by Elsevier B.V.

measures the external surface area and only a proportion of the microporosity that is related to 'crevices in the particle surface, staggered layer edges, voids created by the overlapping of stacked layers and interlayer regions, if the layers separations are sufficiently large' (Rutherford et al., 1997). The determination of the specific surface area and related properties from the nitrogen adsorption isotherm by the BET method is the most common method used to studying smectites. Some comparative studies of these methods have been conducted (Kaufhold et al., 2010; Hegyesi et al., 2017) and they found that the BET model gave a smaller surface areas than expected because nitrogen molecules cannot freely penetrate the interlayer space of the smectites. The accessibility of nitrogen to the smectite layer can be limited by the presence of organic matter (Saidian et al., 2016) and crystalline defects (Suárez Barrios et al., 2001). In addition, the variability of the surface area of smectites is probably determined by the microporosity resulting from the quasi-crystalline overlap region and accessible areas of the interlayer (Kaufhold et al., 2010). The accessibility to the interlayer space depends on the interlayer cations; this was shown in Rutherford et al. (1997) by comparison of a montmorillonite homoionized with different exchangeable cations, in which the Ca^{2+}/Mg^{2+} bentonites had larger specific surface area in comparison to those of Na^{+} bentonites (Kaufhold et al., 2010). Recent studies (Peng et al., 2020) suggest that the specific surface area of bentonites depends on the combination of the previously stated factors.

This study focused on the surface properties, crystal size, and microstructure of a wide group of samples from the three bentonite-producing areas in Spain with the aim of to analyze the influence of the crystal size and crystal defects of smectite, and the microstructure in the microporosity of the bentonites.

2. Experimental

Bentonites from the three bentonite-producing areas in Spain, Cabo de Gata (Almería area), Tajo basin (Madrid and Toledo areas), and Tamame de Sayago (Zamora area), which have different geological origins, are studied here. The geology, mineralogy, and crystal chemistry of these bentonites are described in detail in García-Romero et al. (2019, 2021).

Representative samples from each area (Table 1), denoted as Almería, Tajo, and Tamame, were selected for this study.

- Cabo de Gata area (Almería area): samples COR, CAR-C, CAR-1, CAR-2, CAR-2R, and CAR-3 are from the Cortijo de Archidona quarry; LTBB, LTBV, and LTBN are from Los Trancos quarry; LJ is from Los Jimenez quarry; MM is from the Morrón de Mateo quarry; and SER is from Serrata de Níjar.
- Tajo basin, between Esquivias and Borox (Toledo area): there are samples of bentonites from two different stratigraphic units, from the so-called Pink Clays (ROS, ESB5, RESQ, PB7, and PB10) and from the Green Clays (ESB6, TAJ, and VER).
- Tamame de Sayago (Zamora area): six samples labelled as AR60, BENP, TAM4, TAM5, and TER.

The particle morphology and staking defects were established using high resolution transmission electron microscopy (HR-TEM) at the National Electron Microscopy Centre (Spain). This study was conducted using a JEOL 3000F field-emission microscope with a LaB_6 filament at an acceleration voltage of 300 kV with 0.17 nm point-to-point resolution. Samples for HR-TEM observations were prepared by depositing a drop of diluted clay suspension onto copper grids with a holey carbon film.

X-ray diffraction (XRD) patterns were obtained from samples powdered in agate mortar. A Siemens D-500 XRD diffractometer with Cu Kα radiation and a graphite monochromator was employed, and the samples were scanned from 2° to 65° in steps of 0.05° with a 1 s/step counting time. The X'Pert HighScore Plus V.3 software was used for the pattern analysis.

Table 1
List of the bentonite samples, including location, labelling, approximated purity of smectites (% Sme), and impurities (from XRD data).

AREA	LOCATION	SAMPLE	% Sme	Impurities
ALMERÍA	CORTIJO DE ARCHIDONA	CAR-C	95	Pl
		CAR-1	>95	(Pl)
		CAR-2	>95	(Pl), Q*
		CAR-3	>95	Pl
		CAR-2R	>95	(Pl), Q*
		COR	>95	Pl*
	LOS TRANCOS	LTBB	>95	(Pl)
		LTBV	>95	(Pl), Q*
		LTBN	>95	(Pl)
	LOS JIMÉNEZ	LJ	90	Zeo, (Pl)
	MORRÓN DE MATEO	MM	85	Zeo, (Pl, Crr)
	SERRATA DE NIJAR	SER	95	(Q)
TAJO BASIN	PINK CLAYS	ROS	>95	(Ca)
		ESB5	>95	Q*
		RESQ	>95	Q*
		PB7	>95	Q*
		PB10	>95	Kln*
	GREEN CLAYS	VER	60	Ilt, Q (Kln, Fsp)
		ESB6	65	Ilt, Q (Kln, Fsp)
		TAJ	75	Ilt, Q (Kln, Fsp)
TAMAME		TAM4	85	Q, Alu*
		TAM5	70	Kln, Q*
		TER	55	Q, Kln, (Ms)
		AR60	65	Kln, (Ms, Q), (Fsp)
		BENP	60	Q, Kln, (Ms)

"Impurities" refers to the minerals that appear with the smectite; the order is related to the abundance, starting with the most abundant. Minerals between brackets are <5% in weight, and minerals with * are at trace levels. Alu: alunite, Ca: calcite, Crr: corrensite, Fsp: feldspar, Ilt: illite, Kln: kaolinite, Ms.: muscovite, Pl: plagioclase, Q: quartz, and Zeo: zeolites. Exc. Cat.: Exchangeable cations according García-Romero et al., (2021).

The N_2 adsorption–desorption isotherms at −196 °C were obtained from a static volumetric apparatus (Micromeritics ASAP 2010 adsorption analyser). All samples were pre-treated and analysed in the same way: 0.3 g of raw sample powdered in a manual mortar was out-gassed for 10 h at room temperature, and then for 4 h at 110 °C to reach a lower pressure of 3 μm Hg. The isotherms were obtained following a previously fixed 40-point P/P_0 table, and the reproducibility of the isotherms was checked. The physical adsorption of a gas, N_2 in this case, over the entire exposed surface of a material and the filling of pores is called physisorption, and it is used to measure the total surface area and pore size analysis of nanopores, micropores and mesopores from the first studies of Brunauer et al. (1938). The analysis of the isotherms and the calculations of the surface properties, including the specific surface area (SSA_{BET}), micropore area ($SSA_{\mu p}$) and volume ($V_{\mu p}$), external area (SSA_{Ex}), and mean equivalent pore diameter, were obtained following the classical methods, by the application of the BET equation (Brunauer et al., 1938), and the t-plot (Dubinin and Radushkevich, 1947) and using the Micromeritics software ASAP2010 V3.0.

Statistical analysis was performed using Past software (Hammer et al., 2001). Abbreviations for the mineral names were used according to Whitney and Evans (2010).

3. Results

3.1. Stacking defects and crystal size

Powder XRD patterns of representative samples are shown in Fig. 1; all patterns were asymmetric towards high 2θ values corresponding to hk0 reflections. These characteristic bands of smectites had small differences in position that were related to the di or trioctahedral character. Dioctahedral smectites have 2/3 of the octahedral positions occupied,

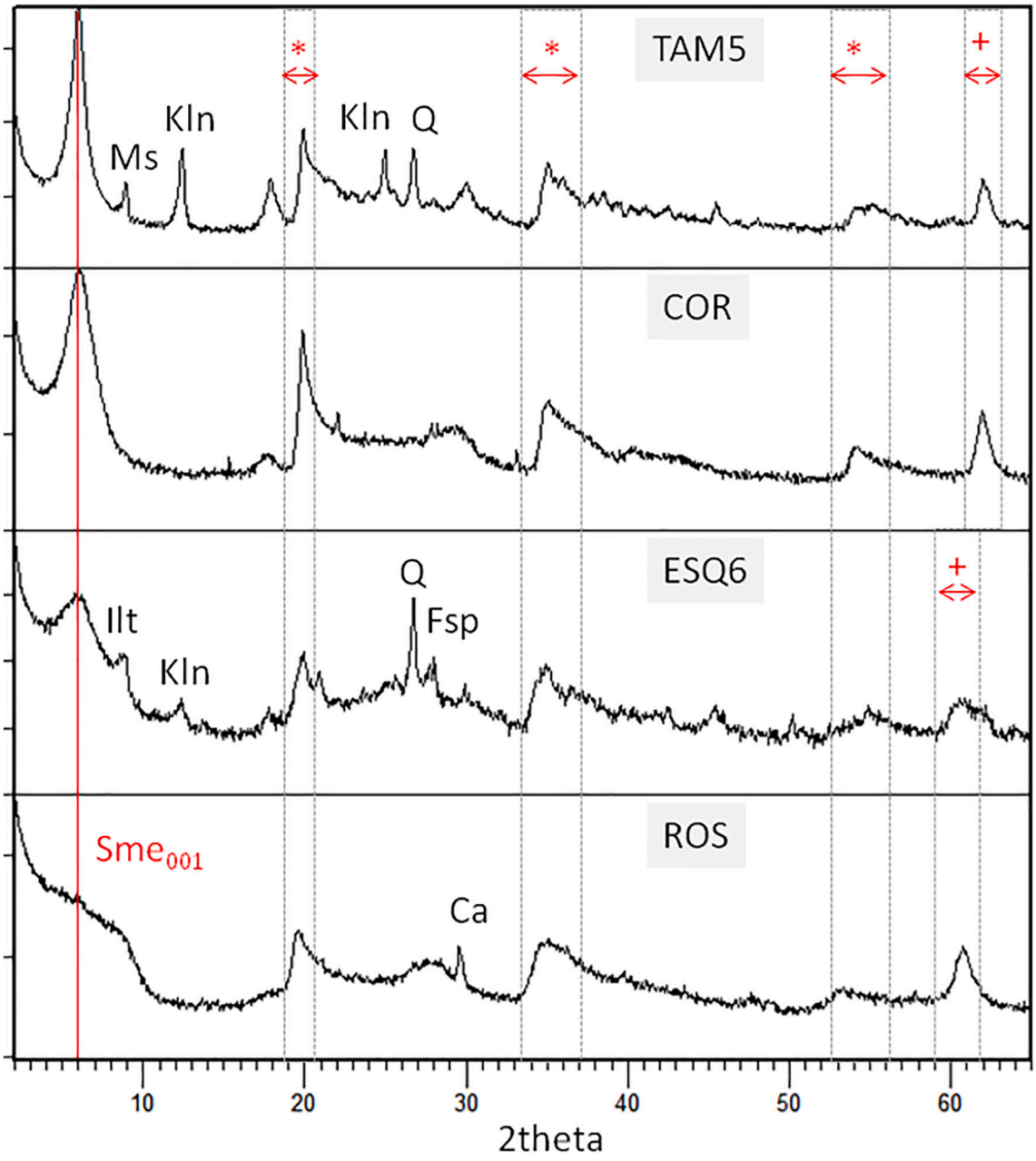

Fig. 1. Powder XRD patterns of representative samples ordered from the lowest crystallinity (with respect to the staking of the layers) at the bottom to the highest crystallinity at the top. TAM5 form Tamame, COR from Almería and ESQ6 and ROS from Tajo. Red line indicates 001 d-spacing of smectite and the regions between black lines indicated with * correspond to hk0 reflection. The band at highest °2theta, indicated with + corresponds to the 060 reflection. (For interpretation of the references to colour in this figure legend, the reader is referred to the web version of this article.)

mainly by Al^{3+} and/or $Fe3^{+}$, while trioctahedral smectites have all octahedral positions occupied, mainly by Mg^{2+}, therefore the dimensions of the lattice are different. This can be deduced from the d-spacing of hk0 reflection, particularly in the 060 reflection because it appears at ~62° 2theta (~0.150 nm) in dioctahedral smectites and at ~61° 2theta (~0.152 nm) in trioctahedral smectites. In the samples here studied, the d-spacing of the 060 reflection is ~0.150 nm in the samples from Almería and Tamame, indicating their dioctahedral character, and at ~0.152 nm in the samples from Tajo indicating that they are trioctahedral smectites. The XRD patterns of the Green Clays from the Tajo had a double 060 peak, whit two maximum at 0.150 nm and ~ 0.152 nm due to illite impurities (dioctahedral) among the trioctahedral smectites.

On the other hand, although all patterns are similar, there are significant differences in the shape of the main 001 reflection, located at ~6° (~1.5 nm). The 001 reflection correspond to the direction of the layer staking in the smectite, as in all phyllosilicates. This peak is narrow and has a high intensity with respect to the other smectite reflections when the smectites is ordered in [001] direction (the stacking direction), such it occurs in the samples from Tamame and Almería (Fig. 1). In contrast, the intensity of the 001 reflection is low, and the peak is broad when the smectite has stacking defects, such as in the XRD-patterns of the Tajo samples. The lack of stacking in the [001] direction of the smectites in the Pink Clays is remarkable; in fact, in the region of higher d-spacings, there is not a 001 reflection. In contrast, there is only one very wide band at lower angles that finishes at ~1.0 nm while the hk0 reflections are similar to those of the other smectites (Fig. 1). This implies that the layers that are diffracting have very low periodicity in this direction, and only very few layers are stacked.

The stacking defects in the smectites are frequent and characteristic of smectites. They are mainly related to their crystal growth process of aggregation via semi-oriented attachment (García-Romero and Suárez, 2018), and they are particularly abundant in the smectite quasi-crystals from Tajo, as observed in the TEM images and the XRD patterns. All observed smectites had numerous stacking defects (Fig. 2), but they were particularly abundant in the samples from Tajo. Fig. 2a shows a smectite particle from Almería (LTBN sample) with few stacking defects and crystal size much larger than those from Tajo (Fig. 2b and c). In contrast, the samples from Green and Pink Clays were characterised by very small size, with very few 2:1 layers stacked and high number of stacking defects (Fig. 2b and c). In contrast, the samples from Green and Pink Clays were characterised by very small size, with very few 2:1 layers stacked and high number of stacking defects (Fig. 2b and c). The differences in the sizes of the crystals of the representative samples is shown in Fig. 3. Smectites from Tajo, particularly the Pink Clays, have high number of stacking defects and the smallest particle size. In contrast, the smectites from Tamame exhibited the largest crystals and the best stacking order among the studied samples.

The powder XRD patterns of the bentonites do not only show the high purity of the samples and the nature of their impurities (see Table 1), the dioctahedral character of the smectites from Almería and Tamame and the trioctahedral character of the Tajo samples, but also indicate the degree of ordering in the layer stacking direction.

3.2. N_2 adsorption–desorption isotherms

The obtained N_2 adsorption–desorption isotherms were similar, some of which are shown in Fig. 4. The form of the isotherms and the hysteresis loops are related to the type of porosity, and the surface properties of the solid can be deduced from the the isotherm (Lowell and Shields, 1984; Rouquerol et al., 1999). According to the International Union of Pure and Applied Chemistry (IUPAC) classification, the first part of the curve, which corresponds to minor relative pressures, can be classified as Type I, which is characterised by the concave curvature towards the abscise axis. This type of N_2 isotherm is characteristic of microporous solids (Thommes et al., 2015). At the highest relative pressures, the obtained isotherms were asymptotic with respect to the ordinate axis, and they did not show limit adsorption at relative pressures close to the unit (Type II isotherms), which is characteristic of capillary absorption in *meso* and macropores. All the isotherms showed hysteresis loops at relative pressures >0.5 owing to the presence of mesopores. According to their form, these hysteresis loops are classified as Type H3 (Thommes et al., 2015). Although all the obtained isotherms had the same type of hysteresis loop, there were remarkable differences among the samples regarding the hysteresis width (Fig. 4). The isotherms of the samples from the Pink Clays and from Almería had the widest hysteresis loops due to a higher condensation of N_2 in mesopores.

The specific surface area, micropore area, external surface area, micropore volumes, and average pore diameters obtained from the isotherms and from the BET equation and the t-plot (Brunauer et al., 1938; Dubinin and Radushkevich, 1947) are listed in Table 2. The SSA_{BET} ranged between 25 and 278 m^2g^{-1} for the BENP and PB7 samples, respectively. In general, the samples can be ordered from the higher to the lower SSA_{BET} as follows: Pink Clays and Green Clays from Tajo, Almería, and Tamame. The micropore area ranged from 6 m^2g^{-1} in sample BENP to 76 m^2g^{-1} in sample PB7, while the external surface area varied from 18 m^2g^{-1} to more than 200 m^2g^{-1} in all the Pink Clay samples. Fig. 5 shows plots of the pore volume versus the average pore diameter for some representative samples of each area. The curves show a variable distribution of pore sizes in each sample. The samples from the same deposit have similar surface properties, with small variations among the samples.

4. Discussion

As shown in Fig. 6, in which the values of specific surface area, micropore area, and external surface area are grouped according to their origin, the samples from the same area have similar values of these variables. The group of samples with small specific surface area are those that came from the Tamame deposit (14–66 m^2g^{-1}). On the other extreme, the samples from the Tajo deposit have the largest specific surface area, and within this group, the samples of the Pink Clays have the highest SSA_{BET} (~270 m^2g^{-1}), followed by the Green Clays (123–179 m^2g^{-1}). The bentonites from the Tajo and Almería areas have been studied previously for potential use in radioactive waste disposal, mainly the so-called FEBEX bentonite that comes from the Cortijo de Archidona (Almería, similar to the CAR samples in this work). Cuevas et al. (1992) studied two representative bentonitic samples from Tajo with high saponite content; they had SSA_{BET} of 149 and 192 m^2g^{-1}, which are slightly below those reported here. SSA_{BET} between 65 and 84 m^2g^{-1} have been found for the samples from Cortijo de Archidona in this study, but values between 32 and 59 m^2g^{-1} were found for natural bentonites with 90% smectites from the same source, which is slightly lower than that of the samples studied here (Fernández et al., 2006; Villar et al., 2008).

The average difference of more than 100 m^2g^{-1} in the SSA_{BET} of the Pink and Green Clays is mainly related to the amount of impurities in the Green Clays (Table 1) because the bentonites of the Green Clays contain non-adsorbent minerals like mica, quartz and feldspars. However, the impurity content is not the only factor that affects the specific surface area. Assuming that the SSA_{BET} of the samples is mainly due the smectite content, we can extrapolate to the theoretical value of SSA_{BET} of each sample for a similar bentonite but with a purity of 100%. With this assumption, the Green Clays have SSA_{BET} in the characteristic range of the Pink Clays or close to them (Table 2). However, the bentonites from

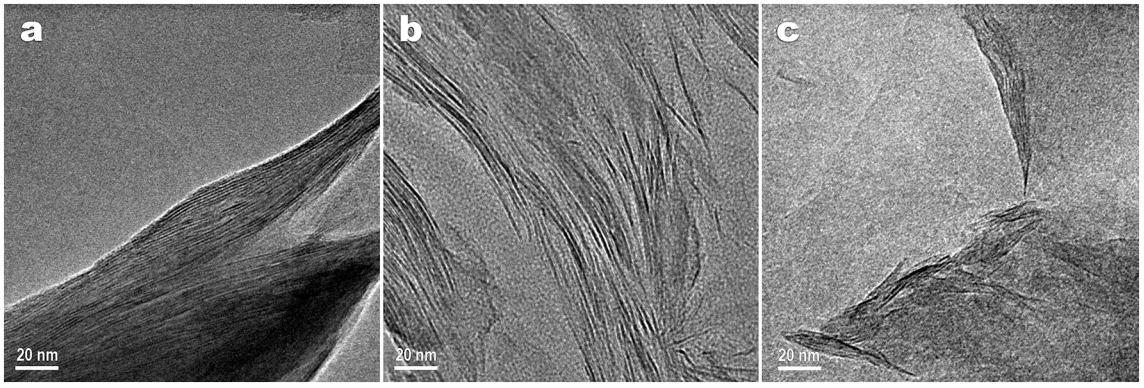

Fig. 2. High-resolution TEM images. a) LTBN sample, b) VER sample, and c) ESB6 sample. The two samples from Tajo (VER and ESB6) show the lattice fringes of smectites with a high number of stacking defects and smaller particle size than LTBN sample.

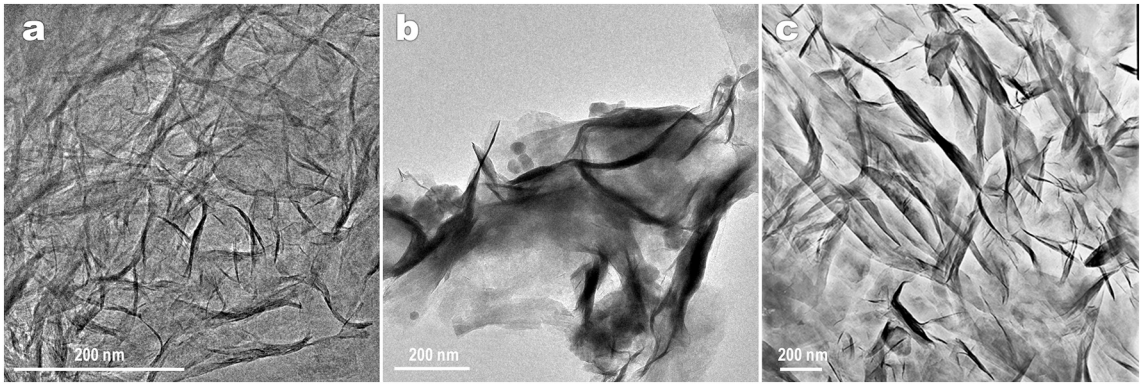

Fig. 3. TEM images showing the general aspects of the a) ROS, b) LTBB, and c) TAM4 samples. Note the smaller laminar particles in the ROS sample and the largest particles in the TAM4 sample.

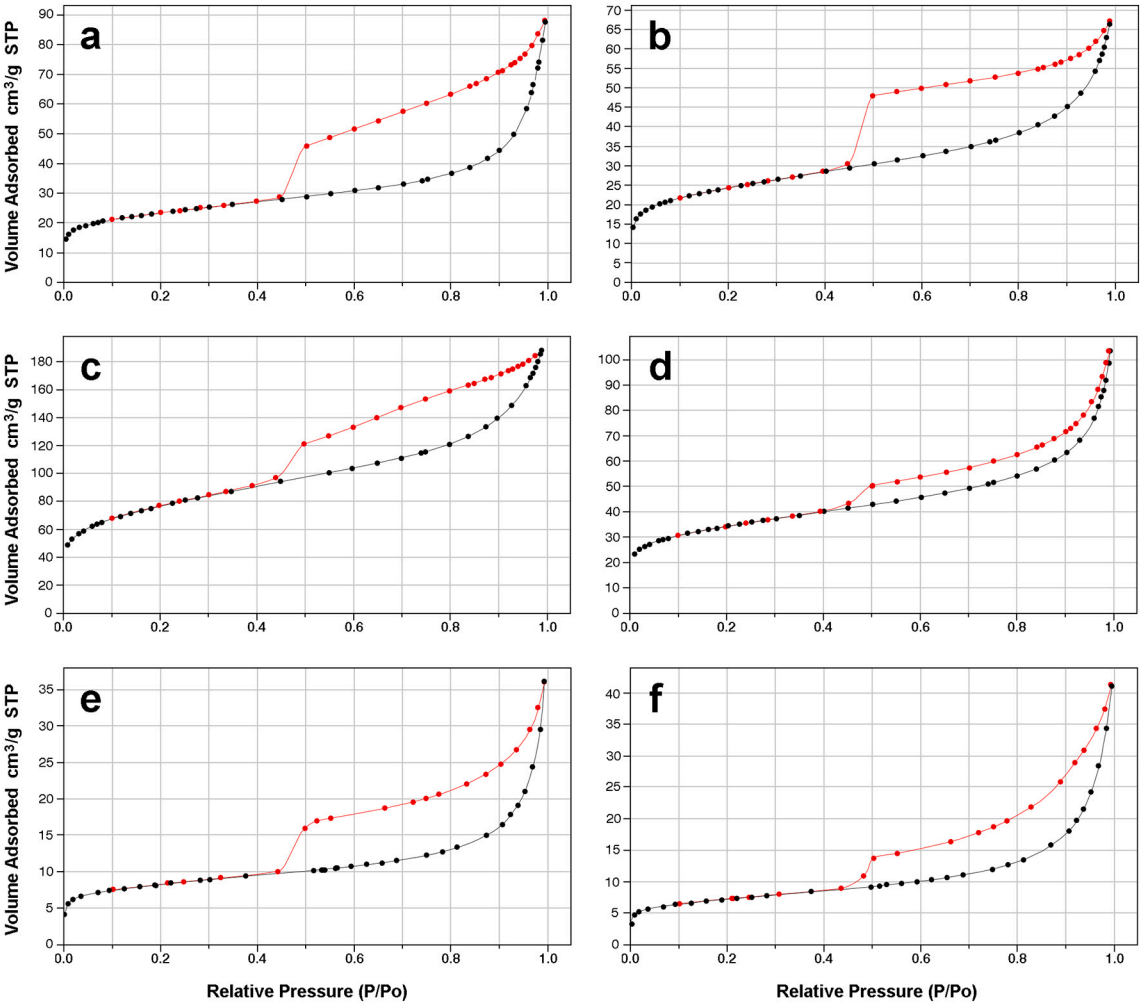

Fig. 4. N_2 adsorption–desorption isotherms of some representative samples: a) CAR-2, b) LJ, c) ROS, d): ESB6, e) TER, f) BENP. The horizontal axis is the relative pressure (P/P_0) which is the equilibrium pressure divided by the saturation pressure.

the Tamame area do not exceed 80 m^2g^{-1}. Neither does the group of samples from Almería; in this case, some samples contain zeolites that also contribute to the SSA_{BET}, but in most cases SSA_{BET} is less than 100 m^2g^{-1}, even for almost pure smectites, such as all the CAR samples. The calculated SSA_{BET} demonstrate that factors other than the amount of impurities affect the specific surface area because the impurity content does not justify the differences among the SSA_{BET} of the studied samples.

There are important differences in the surface properties that cannot be explained by the presence of impurities and, therefore, they must be related to intrinsic properties of the smectites, that are the minerals that contribute to the surface properties of the samples. To explain such differences, the ratio of $SSA_{\mu p}$ to SSA_{Ex} was considered together with the micropore volume and the mean pore diameter (Table 2). The SSA_{Ex} contributes to the SSA_{BET} and it is higher as lower the particle size, being

Table 2
Textural data calculated from the N_2 isotherms.

	SSA_{BET} (m^2g^{-1})	$SSA_{\mu p}$ (m^2g^{-1})	SSA_{Ex} (m^2g^{-1})	$V_{\mu p}$. (m^3g^{-1})	Av. Pore D. (Å)	*BET SSA (m^2g^{-1})
ALMERÍA						
CAR-C	65	22	44	0.0093	53.9	68
CAR-1	67	26	41	0.0111	68.7	71
CAR-2	84	30	54	0.0126	61.6	88
CAR-3	68	27	41	0.0112	56.9	72
CAR-2R	74	26	48	0.0111	61.1	78
COR	74	26	48	0.0133	20.0	78
LTBB	99	37	62	0.0155	53.7	104
LTBV	118	43	75	0.0183	44.6	124
LTBN	82	31	51	0.0131	51.9	86
LJ	86	27	60	0.0115	46.3	96
MM	65	16	49	0.0072	53.2	76
SER	127	47	80	0.0238	20.1	134
TAJO						
ROS	270	62	208	0.0273	42.3	284
ESB5	268	74	194	0.0321	49.6	282
RESQ	267	64	203	0.0280	35.9	281
PB7	278	76	202	0.0393	45.3	293
PB10	209	67	142	0.0346	46.4	220
VER	145	50	93	0.0215	44.3	242
ESB6	123	40	83	0.0168	49.9	189
TAJ	179	68	112	0.0339	20.0	239
TAMAME						
TAM4	66	28	39	0.0139	20.0	78
TAM5	34	14	20	0.0062	19.0	48
TER	28	10	18	0.0049	19.9	51
AR60	31	11	20	0.0052	19.9	48
BENP	25	6	19	0.0030	20.0	42

SSA_{BET}: SSA measured by the BET method (Brunauer et al., 1938), $SSA_{\mu p}$: micropore area, SSA_{Ex}: external surface area, $V_{\mu p}$: micropore volume, Av. pore D.: Average pore diameter. * SSA_{BET}: SSA calculated for 100% smectite.

this inverse relation higher for laminar particles like smectites. In these samples, the SSA_{Ex} contributes more to the SSA_{BET}, as shown in Fig. 6, but not in the same way in all samples. The values of $SSA_{\mu p}$ and SSA_{Ex} have a high positive correlation (Fig. 7), with $R = 0.847$ (Pearson correlation coefficient), this R value improves slightly (0.852) when the samples with zeolite impurities (LJ and MM) are not considered, because those minerals contribute to the microporosity. However, when the Pink Clay samples are not considered, the correlation coefficient between $SSA_{\mu p}$ and was close to unity (0.955). Pink Clays do not follow the general trend (Fig. 7) mainly because of their external surface area, which is between 142 m^2g^{-1} and 208 m^2g^{-1}. This high external surface area of the Pink Clays is related to their small particle size (Fig. 3) (de Santiago Buey et al., 2000). The samples with the lowest SSA_{Ex} are those from Tamame, and they have the biggest laminar particles. The order of particle size, from the smallest to the biggest, is Pink Clays, Green Clays, Almería, and Tamame, and this exact order is the same for the SSA_{Ex} values, but in this case from the biggest to the smallest, due to the inverse relation between particle size and external surface area. The influence of the dimensions of the elemental silicate 2:1 layers has been discussed previously (Aylmore and Quirk, 1967); larger crystals dimensions result in lower surface areas in the bentonites, while the crystal size in [001] direction, or the number of layers per stack, should play a subordinate role according to Kaufhold et al. (2010) and Peng et al. (2020).

In addition to the influence of the particle size, the arrangement of both the elementary 2:1 layers in quasi-crystals and the arrangement of the individual particles must be considered (Schoonheydt, 1994; Michot and Villiéras, 2006). The arrangement of the elementary 2:1 layers in [001], the staking direction, can be deduced from the size and the width of the 001 reflection in the XRD powder patterns. According to this, the samples can be classified from "very high crystallinity", for samples with a narrow, intense, and well-defined 001 reflection, to "very low crystallinity", for samples showing very broad diffraction effects in the region of high d-spacing. Samples can be classified as well into four categories that are coincident with the location of the deposits: very high crystallinity (Tamame), high crystallinity (Almería), low crystallinity (Green Clays from Tajo), and very low crystallinity (Pink Clays from Tajo). The particle size and the staking order follow this same order from the largest to the smallest (Fig. 3) which corresponds with an increase in the SSA_{BET}.

The Green and Pink Clays differ in macroporosity (Fig. 5), but the layer size and abundance of stacking defects (Figs. 2 and 3) are similar; thus, the difference in the SSA_{BET} is mainly related to the impurity content, as has been previously shown. The high values of both $SSA_{\mu p}$ and SSA_{Ex}, and consequently the high SSA_{BET} values, of the bentonites from Tajo were mainly related to their small particle size and their crystallinity. The samples from Tajo are those which have the best surface properties, highest values of SSA_{BET}, $SSA_{\mu p}$, and SSA_{Ex} because they have the smallest particle size and very low crystallinity due to the abundance of staking defects.

Fig. 8 shows the influence of particle size, the staking defects, and the microstructure in the surface properties of these laminar minerals. The external surface surrounding the particles, the interlayer or intracrystalline microporosity that is accessible to the N_2 at the edge of the particles, and the microporosity at the edge due to staking defects are schematized (Fig. 8a). In Fig. 8b it is shown how two particles with half lateral extension double their microporosity. The lateral dimension of the laminar particles influences the SSA_{BET}, and smaller particle sizes yielded higher surface areas, mainly because of increased microporosity. As the interlayer space is partially accessible to the N_2 molecules (Kaufhold et al., 2010); therefore, as the lateral dimensions decreases, the proportion of edge particles and consequently accessible area increase (Fig. 8). When the external surface area of the edge increases, the proportion of edge microporosity related to stacking defects also increases (Fig. 8b). In contrast, the external surface area is higher when the particles have few elemental 2:1 units stacked because the number of basal surfaces exposed to the N_2 molecules is higher (Fig. 8c). The imperfect parallel stacking of 2:1 layers in the crystal due to the crystal growth by semi-oriented attachment (García-Romero and Suárez, 2018) or the laminar particles in the aggregate (as shown in Fig. 8d) can also generate microporosity and mesoporosity.

The microporosity related to the crystalline defects, both for stacking and for edge ordering, are common in the saponites from Tajo, as shown in Fig. 2, and is another cause of the high microporosity of these samples, together with their small particle size (Fig. 3). The influence of particle size on the microporosity is related to the crystalline structure due to the different accessibility of N_2 to the interior of the crystals. The existence of microstructural microporosity related to the arrangement of the crystals was also reported for sepiolite by Suárez and García-Romero (2012).

The pore size distribution (Fig. 5) varied between samples. Although in all cases there are pores throughout the full-size range, there are distinct common characteristics for each group. The samples from Almería have lower microporosity and maximums in the highest sizes of mesoporosity. For example, the LTBN sample has its maximum value of pore volume at an equivalent pore diameter of 35 nm, and the MM sample has its maximum value in the macropore range (Fig. 5). Samples from Tajo showed the highest pore volume for lower pore sizes (Fig. 5), and accordingly the highest values of $SSA_{\mu p}$, and a maximum in the mesopore range, between 10 and 20 nm. In contrast, the samples from Tamame have very low microporosity, and the maximum pore volume is in the macropore range.

A hierarchical analysis performed using Ward's method, which considers all data obtained from the N_2 isotherms, grouped the samples according to their origin. This agrees with Dogan et al. (2007), who affirm that the textural properties are characteristic of each clay deposit.

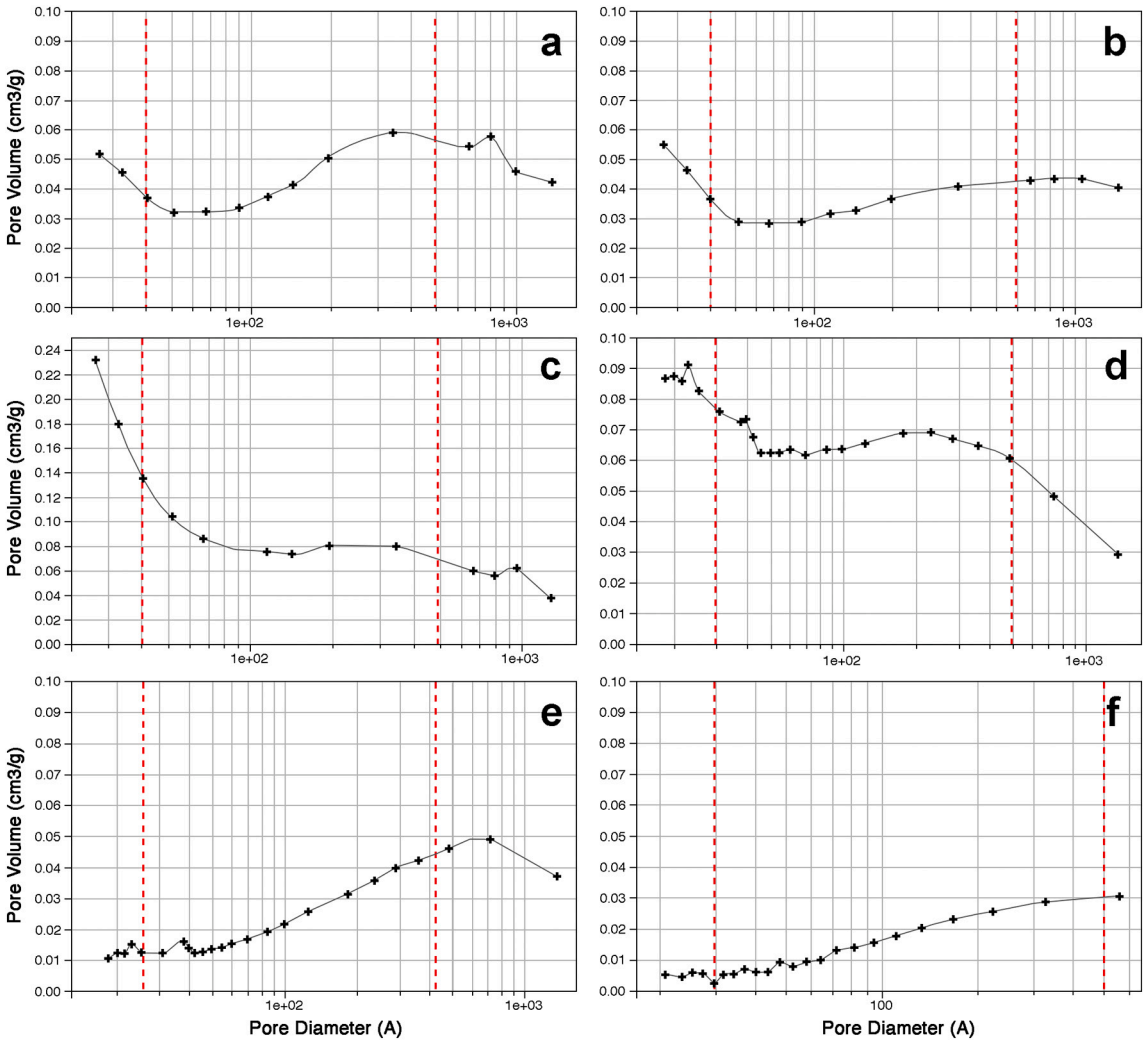

Fig. 5. Pore diameter distribution of some representative samples: a) LTBN, b) MM, c) RESQ, d): TAJ, e) AR60, f) TER. The discontinuous red lines delimit the micropores, mesopores and macropores. The vertical scale is the same for all samples except for RESQ. (For interpretation of the references to colour in this figure legend, the reader is referred to the web version of this article.)

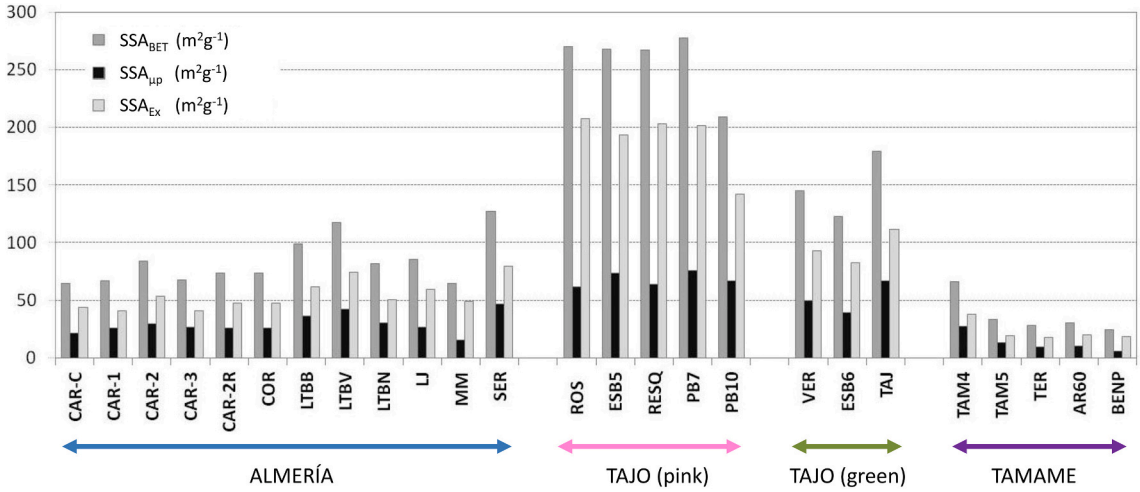

Fig. 6. Graphical representation of the SSA$_{BET}$, SSA$_{\mu p}$, and SSA$_{Ex}$ values of the samples ordered by areas of provenance.

Fig. 9 shows the clusters obtained considering to the external surface area; the samples were grouped almost perfectly according to their geological origin and, as shorter the distance higher the similarity. The hierarchy of clusters first separated the Pink Clays from the rest because of their different particle sizes. The second group was subdivided into three groups that correspond to Tamame, Almería, and Green Clays

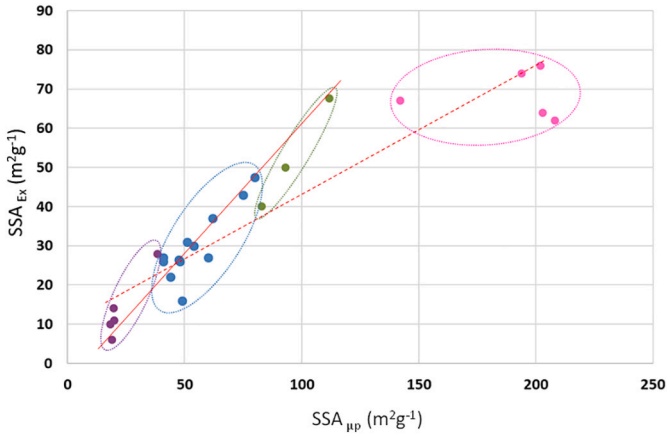

Fig. 7. Binary plot of $SSA_{\mu p}$ and SSA_{Ex}. The red and continuous line is the linear regression with all the samples, while the red and discontinuous line is the linear regression without the Pink Clays. (For interpretation of the references to colour in this figure legend, the reader is referred to the web version of this article.)

together with SER, and LTBV bentonites. The samples were grouped according to their common characteristics, such as particle size, stacking defects, and microstructure, that influence the surface properties. These are characteristic of each deposit because they are related to their genesis.

5. Conclusions

A comparative study of a wide group of very pure bentonites with similar exchangeable cations, were studied without pre-treatments that may affect the microstructure. This allowed the analysis of the influence of crystalline defects, particle size, and microstructure on the surface properties of the samples. The samples came from different deposits in the three areas in which bentonites are mined in Spain. Each of these areas has their own and characteristic microstructural features that are related to their geological origin. The size of the crystals and the particles (i.e. aggregates), the abundance of crystalline defects, and the arrangement of the particles are different and characteristic of each deposit, and they affect the surface properties.

This comparative study shows that the crystal size and crystalline defects of smectites influence the surface properties of bentonite

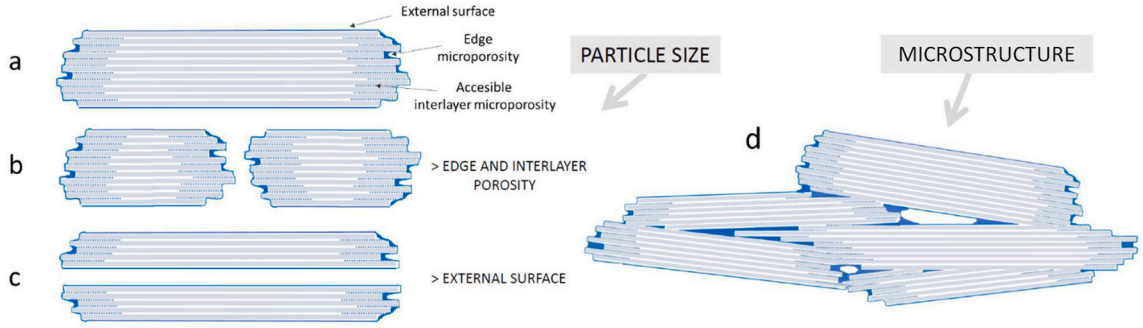

Fig. 8. Schematic representation of the N_2 adsorption (in blue) on smectite crystals and particles. Comparison among different sized particles showing the influence of the lateral extension of the layers and the number of 2:1 stacked layers and micro and mesoporosity due to the arrangement of the crystals forming particles. (For interpretation of the references to colour in this figure legend, the reader is referred to the web version of this article.)

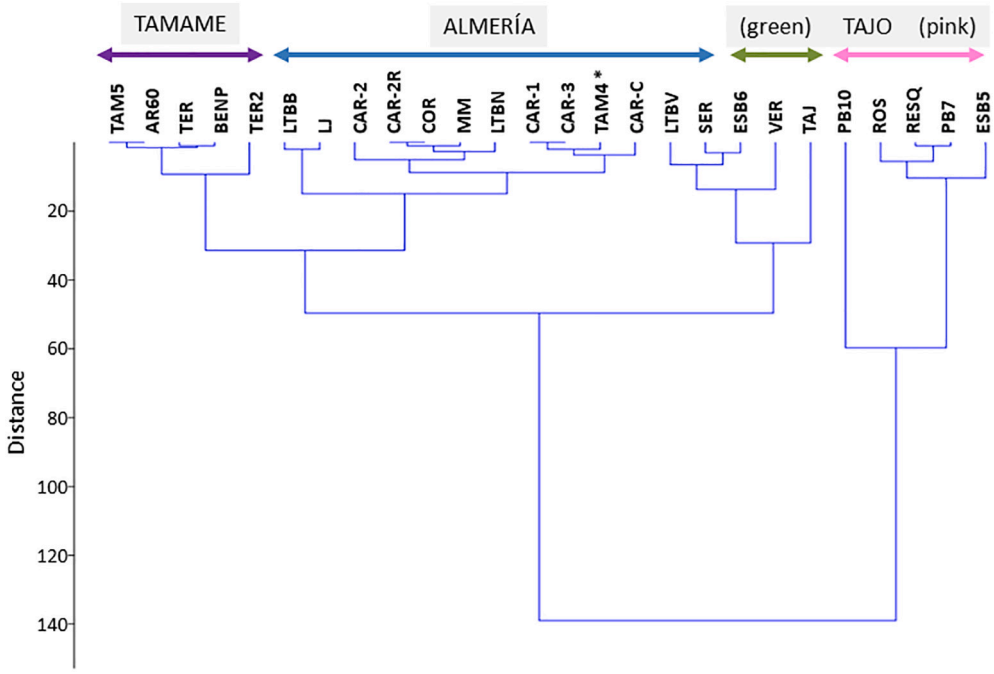

Fig. 9. Grouping of the samples in different clusters considering the external surface area of the samples.

considerably more than previously thought. Owing to the partial accessibility of N_2 to the interior of the interlayer space of the particles, the lateral dimension of the crystals considerably influences the measured microporosity, while the size in the [001] direction influences the external surface area. This is why the samples from Tajo, both the Green and Pink Clays, have the highest values of micropore and external surface area. In addition, the microporosity is also related to the stacking defects because the stacking of elemental 2:1 layers with small angles produces accessible micropores, as has been previously reported (Kaufhold et al., 2010).

The microporosity is not restricted to the crystal or quasi-crystal but also depends on the arrangement of the crystals into aggregates; in other words, it also depends on the microstructure because subparallel arrangements with low angles produce microporosity, similar to that produced by the 2:1 layers.

N_2 adsorption studies showed that the bentonites have pores in the full range of sizes: smaller micropores of only a few angstroms (related to the crystalline structure of the interior of the interlayer and at the quasi-crystal edge), *meso*pores due to the microstructure, and macropores in the micrometric range. However, although the amounts of micro, meso, and macropores varied between samples, they are similar and characteristic for samples from the same geological areas.

Declaration of Competing Interest

The authors declare that they have no known competing financial interests or personal relationships that could have appeared to influence the work reported in this paper.

Acknowledgments

This work has been funded by Spanish Junta de Castilla y León (grant SA0107P20) and Ministerio de Ciencia e Innovación (grant number PID-2019-106504RB).

References

Adem, H.H., Vanapalli, S.K., 2015. Review of methods for predicting in situ volume change movement of expansive soil over time. J. Rock Mech. Geotech. Eng. 7 (1), 73–86. https://doi.org/10.1016/j.jrmge.2014.11.002.

Aylmore, L.A.G., Quirk, J.P., 1967. The micropore size distributions of clay mineral systems. J. Soil Sci. 18, 1–17. https://doi.org/10.1111/j.1365-2389.1967.tb01481.x.

Brunauer, S., Emmett, P.H., Teller, E., 1938. Adsorption of gases in multimolecular layers. J. Am. Chem. Soc. 60, 309–319. https://doi.org/10.1021/ja01269a023.

Cuevas, J., Medina, J.A., Leguey, S., 1992. Saponitic clays from the Madrid basin: Accessory-minerals influence in hydrothermal reactivity. Appl. Clay Sci. 7, 185–199. https://doi.org/10.1016/0169-1317(92)90039-P.

de Santiago Buey, C., Suárez Barrios, M., García-Romero, E., Doval Montoya, M., 2000. Mg-rich smectite "precursor" phase in the Tagus Basin, Spain. Clay Clay Miner. 48, 366. https://doi.org/10.1346/CCMN.2000.0480307.

Dogan, M., Dogan, A.U., Yesilyurt, F.I., Alaygut, D., Buckner, I., Wurster, D.E., 2007. Baseline studies of the Clay Minerals Society special clays: specific surface area by the Brunauer Emmett Teller (BET) method. Clay Clay Miner. 55, 534–541. https://doi.org/10.1346/CCMN.2007.0550508.

Dubinin, M.M., Radushkevich, L.V., 1947. Equation of the Characteristic Curve of Activated Charcoal, Proceedings of the Academy of Sciences. Physical Chemistry Section, U.S.S.R, 55, pp. 331–333, 1947.

Fernández, R., Cuevas, J., Sánchez, L., de la Villa, R.V., Leguey, S., 2006. Reactivity of the cement–bentonite interface with alkaline solutions using transport cells. Appl. Geochem. 21, 977–992. https://doi.org/10.1016/j.apgeochem.2006.02.016.

García-Romero, E., Suárez, M., 2018. A structure-based argument for non-classical crystal growth in natural clay minerals. Mineral. Mag. 82, 171–180. https://doi.org/10.1180/minmag.2017.081.031.

García-Romero, E., María Manchado, E., Suárez, M., García-Rivas, J., 2019. Spanish bentonites: a review and new data on their geology, mineralogy, and crystal chemistry. Minerals 9, 696. https://doi.org/10.3390/min9110696.

García-Romero, E., Lorenzo, A., García-Vicente, A., García-Rivas, J., Morales, J., Suárez, M., 2021. On the structural formula of smectites: a review and new data on the influence of the exchangeable cations. J. Appl. Crystallogr. 54, 251–262. https://doi.org/10.1107/S1600576720016040.

Hammer, Ø., Harper, D.A.T., Ryan, P.D., 2001. PAST: Paleontological statistics software package for education and data analysis. Palaeontol. Electron. 4 (1) (9pp).

Hegyesi, N., Vad, R.T., Pukánszky, B., 2017. Determination of the specific surface area of layered silicates by methylene blue adsorption: the role of structure, pH and layer charge. Appl. Clay Sci. 146, 50–55. https://doi.org/10.1016/j.clay.2017.05.007.

Jeon, I., Nam, K., 2019. Change in the site density and surface acidity of clay minerals by acid or alkali spills and its effect on pH buffering capacity. Sci. Rep. 9 https://doi.org/10.1038/s41598-019-46175-y.

Jlassi, K., Krupa, I., Chehimi, M.M., 2017. Overview: Clay preparation, properties, modification. In: Jlassi, K., Chehimi, M.M., Thomas, S. (Eds.), Clay-Polymer Nanocomposites. Elsevier, pp. 1–28. https://doi.org/10.1016/B978-0-323-46153-5.00001-X.

Jones, L.D., Jefferson, I., 2012. Expansive soils, 516. In: Burland, J., Chapman, T., Skinner, H., Brown, M. (Eds.), ICE Manual of Geotechnical Engineering. Volume 1 Geotechnical Engineering Principles, 517 Problematic Soils and Site Investigation. ICE Publishing, London, pp. 413–441.

Kaufhold, S., Dohrmann, R., Klinkenberg, M., Siegesmund, S., Ufer, K., 2010. N2-BET specific surface area of bentonites. J. Colloid Interface Sci. 349, 275–282. https://doi.org/10.1016/j.jcis.2010.05.018.

Kloprogge, J.T., Duong, L.V., Frost, R.L., 2005. A review of the synthesis and characterisation of pillared clays and related porous materials for cracking of vegetable oils to produce biofuels. Environ. Geol. 47, 967–981. https://doi.org/10.1007/s00254-005-1226-1.

Komadel, P., Madejová, J., Bujdák, J., 2005. Preparation and properties of reduced-charge smectites – a review. Clay Clay Miner. 53, 313–334. https://doi.org/10.1346/CCMN.2005.0530401.

Lowell, S., Shields, J.E., 1984. Adsorption isotherms. In: Powder Surface Area and Porosity. Springer, Dordrecht.

Michot, L.J., Villiéras, F., 2006. Surface area and porosity. In: Bergaya, F., Theng, B.K.G., Lagaly, G. (Eds.), Developments in Clay Science. Elsevier, pp. 965–978. https://doi.org/10.1016/S1572-4352(05)01035-4.

Navarro, V., Asensio, L., De la Morena, G., Gharbieh, H., Alonso, J., Pulkkanen, V.-M., 2020. From double to triple porosity modelling of bentonite pellet mixtures. Eng. Geol. 274 https://doi.org/10.1016/j.enggeo.2020.105714 art. no. 105714.

Okada, T., Seki, Y., Ogawa, M., 2014. Designed nanostructures of clay for controlled adsorption of organic compounds. J. Nanosci. Nanotechnol. 14, 2121–2134. https://doi.org/10.1166/jnn.2014.8597.

Peng, L., Chen, B., Zhao, Y., 2020. Quantitative characterization and comparsion of bentonite microstructure by small angle X-ray scattering and nitrogen adsorption. Constr. Build. Mater. 262, 120863. https://doi.org/10.1016/j.conbuildmat.2020.120863.

Přikryl, R., Weishauptová, Z., 2010. Hierarchical porosity of bentonite-based buffer and its modification due to increased temperature and hydration. Appl. Clay Sci. 47 (1–2), 163–170. https://doi.org/10.1016/j.clay.2009.10.005.

Rouquerol, F., Rouquerol, J., Sing, K., 1999. Adsorption by Powders and Porous Solids. Academic Press, London.

Rutherford, D.W., Chiou, C.T., Eberl, D.D., 1997. Effects of exchanged cation on the microporosity of montmorillonite. Clay Clay Miner. 45, 534–543. https://doi.org/10.1346/CCMN.1997.0450405.

Saidian, M., Godinez, L.J., Prasad, M., 2016. Effect of clay and organic matter on nitrogen adsorption specific surface area and cation exchange capacity in shales (mudrocks). J. Nat. Gas Sci. Eng. 33, 1095–1106. https://doi.org/10.1016/j.jngse.2016.05.064.

Schoonheydt, R., 1994. Clay mineral surfaces. In: Vaughan, D., Patrick, R. (Eds.), Minerals Surfaces. Clapman and Hall, London, pp. 303–332.

Suárez Barrios, M., de Santiago Buey, C., García-Romero, E., Martín Pozas, J.M., 2001. Textural and structural modifications of saponite from Cerro del Aguila by acid treatment. Clay Miner. 36, 483–488.

Suárez, M., García-Romero, E., 2012. Variability of the surface properties of sepiolite. Appl. Clay Sci. 67–68, 72–82. https://doi.org/10.1016/j.clay.2012.06.003.

Sun, H., Mašín, D., Najser, J., Neděla, V., Navrátilová, E., 2020. Fractal characteristics of pore structure of compacted bentonite studied by ESEM and MIP methods. Acta Geotech. 15 (6), 1655–1671. https://doi.org/10.1007/s11440-019-00857-z.

Thommes, M., Kaneko, K., Neimark, A.V., Olivier, J.P., Rodriguez-Reinoso, F., Rouquerol, J., Sing, K.S.W., 2015. Physisorption of gases, with special reference to the evaluation of surface area and pore size distribution (IUPAC Technical Report). Pure Appl. Chem. 87 https://doi.org/10.1515/pac-2014-1117.

Vicente, M.A., Trujillano, R., Ciuffi, K.J., Nassar, E.J., Korili, S.A., Gil, A., 2010. Pillared clay catalysts in green oxidation reactions. In: Raquel, Vicente, Angel, Miguel (Eds.), Gil, Antonio, Korili, Sophia A., Trujillano. Pillared Clays and Related Catalysts, Springer New York, New York, NY, pp. 301–318. https://doi.org/10.1007/978-1-4419-6670-4_11.

Vicente, M.A., Gil, A., Bergaya, F., 2013. Pillared clays and clay minerals. In: Lagaly, G. (Ed.), Bergaya, F. Elsevier, Developments in Clay Science, pp. 523–557. https://doi.org/10.1016/B978-0-08-098258-8.00017-1.

Villar, M.V., Lloret, A., 2004. Influence of temperature on the hydro-mechanical behaviour of a compacted bentonite. Appl. Clay Sci. 26 (1–4), 337–350.

Villar, M.V., Sánchez, M., Gens, A., 2008. Behaviour of a bentonite barrier in the laboratory: Experimental results up to 8 years and numerical simulation. Phys. Chem. Earth Parts A/B/C 33, S476–S485. https://doi.org/10.1016/j.pce.2008.10.055.

Whitney, D.L., Evans, B.W., 2010. Abbreviations for names of rock-forming minerals. Am. Mineral. 95, 185–187. https://doi.org/10.2138/am.2010.3371.
Yamada, H., Tamura, K., Watanabe, Y., Iyi, N., Morimoto, K., 2011. Geomaterials: their application to environmental remediation. Sci. Technol. Adv. Mater. 12, 064705 https://doi.org/10.1088/1468-6996/12/6/064705.
Zhang, F., Ye, W.M., Chen, Y.G., Chen, B., Cui, Y.J., 2016. Influences of salt solution concentration and vertical stress during saturation on the volume change behavior of compacted GMZ01 bentonite. Eng. Geol. 207, 48–55.